Limits to the Inversion of HF Radar Backscatter for Ocean Wave Measurement

LUCY R. WYATT

Sheffield Centre for Earth Observation Science, Applied Mathematics Department, University of Sheffield, Sheffield, United Kingdom

(Manuscript received 26 April 1999, in final form 20 December 1999)

ABSTRACT

The power spectrum of backscatter from the ocean surface at HF radio frequencies is characterized by two large peaks called the first-order Bragg peaks. These are surrounded by a continuum due to second-order effects. The power spectrum can be described in low to moderate sea states by a nonlinear integral equation relating it to the ocean wave directional spectrum. Inverting this equation provides an estimate of the directional spectrum. A number of inversion methods have been published. In this paper, the Wyatt method is discussed. This method uses the part of the backscatter power spectrum that surrounds the larger Bragg peak. An extension of the method to include the spectrum around the weaker peak is discussed, and some improvements in the solution are demonstrated. Until recently, all published work in this area concerned solutions to a linearized version of the equation. The second extension presented here tackles the nonlinear problem but points out the limitations of the approach and shows that improvements to the solution with this or any other method are likely to be minor. Of more importance is the limitation of second-order theory in high sea states, particularly at the higher radio frequencies used at the moment in operational systems. A theory to describe the backscattered signal in these circumstances is a major challenge for the future.

1. Introduction

High frequency (HF) radars transmit high frequency (HF 3–30 MHz) radio waves that are scattered from ocean waves in all directions, with some scattered toward the radar receiver. The largest contribution to the signal at the receiver has been shown (Crombie 1955; Barrick 1972) to be due to scatter from ocean waves of half the radio wavelength traveling directly toward or away from the radar (when the transmit and receive sites are collocated), according to whether the wind is blowing in the half plane toward or away from the radar. This produces a peak in the Doppler power spectrum of the demodulated backscattered signal at a frequency equal to the ocean wave frequency of this Bragg-matched wave. This frequency is positive if the wave is propagating toward the radar, and vice versa. There is a second, usually smaller, peak in the Doppler spectrum at minus the frequency of the larger peak. These peaks can be seen between the two pairs of dashed lines in Fig. 1a. These peaks are shifted in frequency if there is a surface current present. This shift is used to measure surface currents (see, e.g., Paduan and Graber 1997). These peaks are referred to as first-order peaks because they can be described by the first-order solution of a perturbation analysis of the interaction between electromagnetic and hydrodynamic waves. The rest of the power spectrum comprises a continuum, referred to as the second-order part of the spectrum, and a noise floor. In this paper, the second-order parts of the spectrum on either side of the two first-order peaks are referred to as sidebands, and there are four of these in each spectrum. The sidebands on the zero Doppler side of the first-order peaks are referred to as inner sidebands and the others as outer sidebands.

A number of approaches have been developed to provide a theoretical formulation for the power spectrum in terms of the ocean wave spectrum (Barrick and Weber 1977; Robson 1984; Walsh and Srivastava 1987). The perturbation solution developed by Barrick (1971) and Barrick and Weber (1977) is most commonly used and is the basis of the discussion in this paper.

A number of different radar systems have been used for wave measurement. In this paper, the PISCES (Shearman and Moorhead 1988), the OSCR (Wyatt and Ledgard 1996), and the WERA (Gurgel et al. 1999) radars will be mentioned. The PISCES operates in the lower half of the HF band (4–18 MHz) and was designed for wave measurement to ranges of 150 km from the coast. The OSCR and WERA both operate at higher HF frequencies (25–30 MHz), and OSCR was designed specifically for surface current monitoring within 40 km of

Corresponding author address: Dr. Lucy R. Wyatt, Sheffield Centre for Earth Observation Science, Applied Mathematics Department, The University of Sheffield, Hounsfield Road, Sheffield S3 7RH United Kingdom.
E-mail: L.Wyatt@sheffield.ac.uk

© 2000 American Meteorological Society

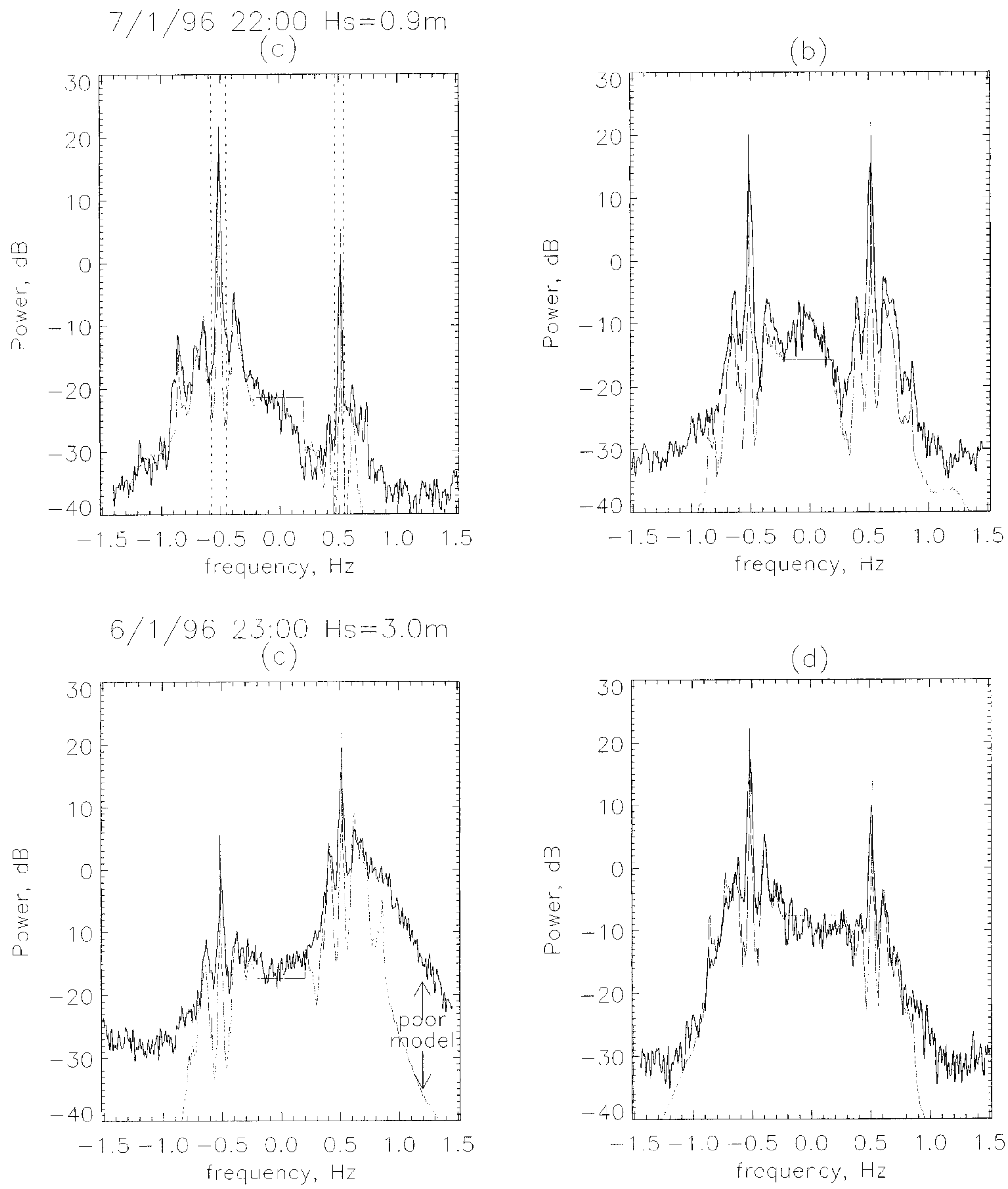

FIG. 1. Doppler spectra measured by OSCR (darker line) compared with spectra simulated with buoy data (lighter line). Date, time, and significant wave heights are shown above each pair. (a) Low significant wave height, energy propagating toward the radar, and (b) energy propagating across the radar beam; (c) high significant wave height, energy propagating toward the radar, showing the discrepancy between theory and measurement, and (d) energy propagating across the radar beam.

the coast. These are all phased array systems for which the problem of extracting wave measurements is rather easier than is the case for compact antenna systems of the CODAR type (Lipa et al. 1990).

a. Barrick's equations

Full mathematical details for the analysis of second-order ocean wave interactions can be found in the work of Weber and Barrick (1977), Barrick and Weber (1977), Lipa and Barrick (1986), and Holden and Wyatt (1992). The latter two deal with the solution in the case of finite depth from which the Weber and Barrick work can be derived as the limit of deep water. The second-order electromagnetic analysis is referred to in Lipa and Barrick (1986) and Barrick (1971) and is based on the method of Rice (1951).

The resulting equations describe the relationship be-

TABLE 1. Parameters used in the simulations.

CASE	Radar frequency (MHz)	Beam 1	Beam 2	Wind speed (m s^{-1})	Wind direction	Swell relative amplitude	Swell direction
1	25.4	5°	115°	9	70°	1.0	220°
2	25.4	5°	115°	9	70°	2.0	220°
3	25.4	5°	115°	9	70°	5.0	220°
4	25.4	5°	115°	9	70°	10.0	220°
5	27.0	0°	70°	10	90°	0.0	—
6	27.0	0°	70°	10	90°	0.5	90°
7	27.0	0°	70°	10	90°	0.5	180°
8	27.0	0°	70°	10	90°	0.5	270°

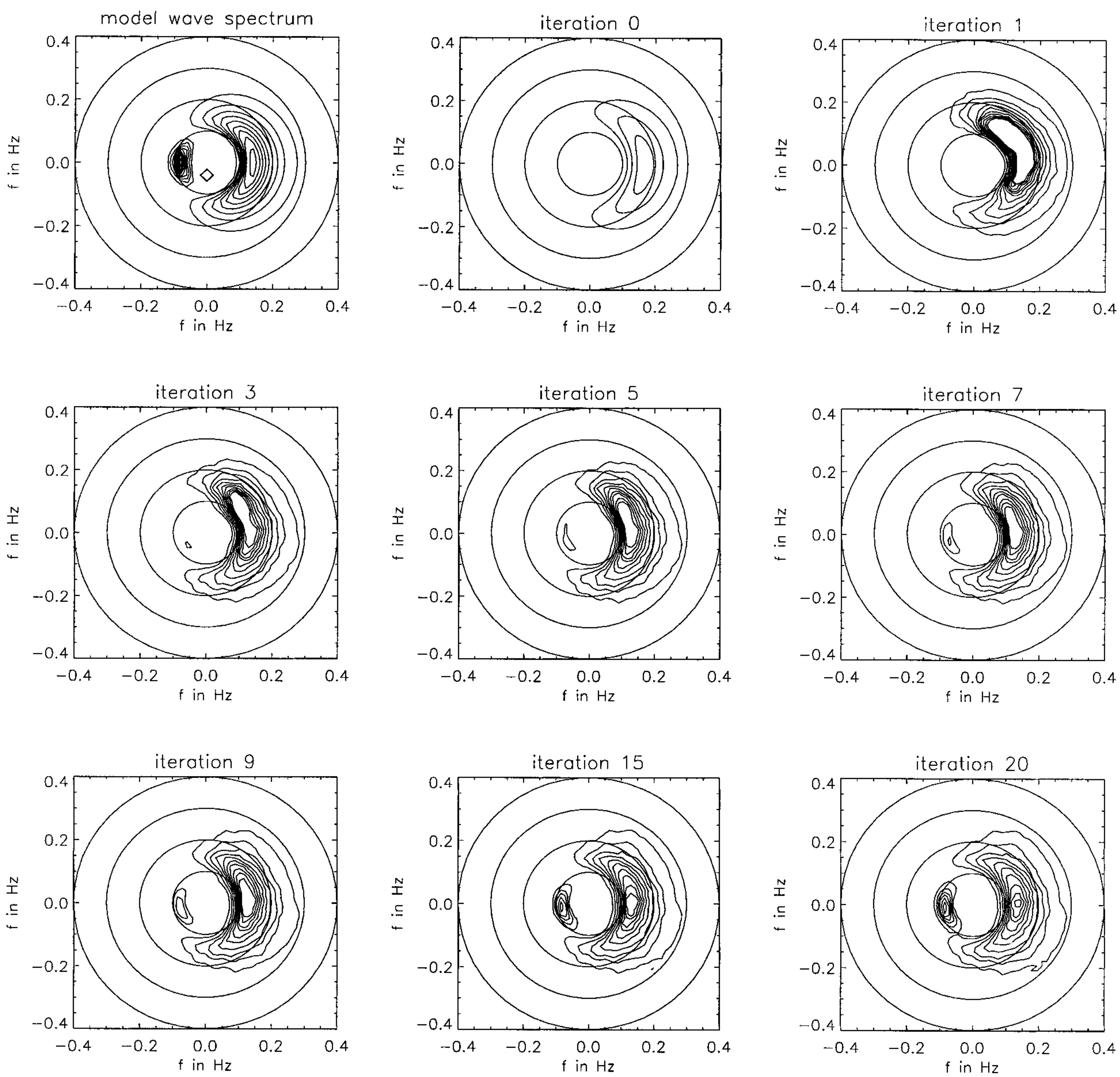

FIG. 2. The development of the estimated directional spectrum during the inversion process plotted in polar form. The number of iterations for each inverted spectrum is shown. Circles are drawn at frequencies of 0.1, 0.2, and 0.3 Hz to aid comparison. Ten linear levels are contoured at increments of 0.1 of the maximum. Each spectrum is scaled with respect to the maximum energy density in the modeled spectrum shown top left.

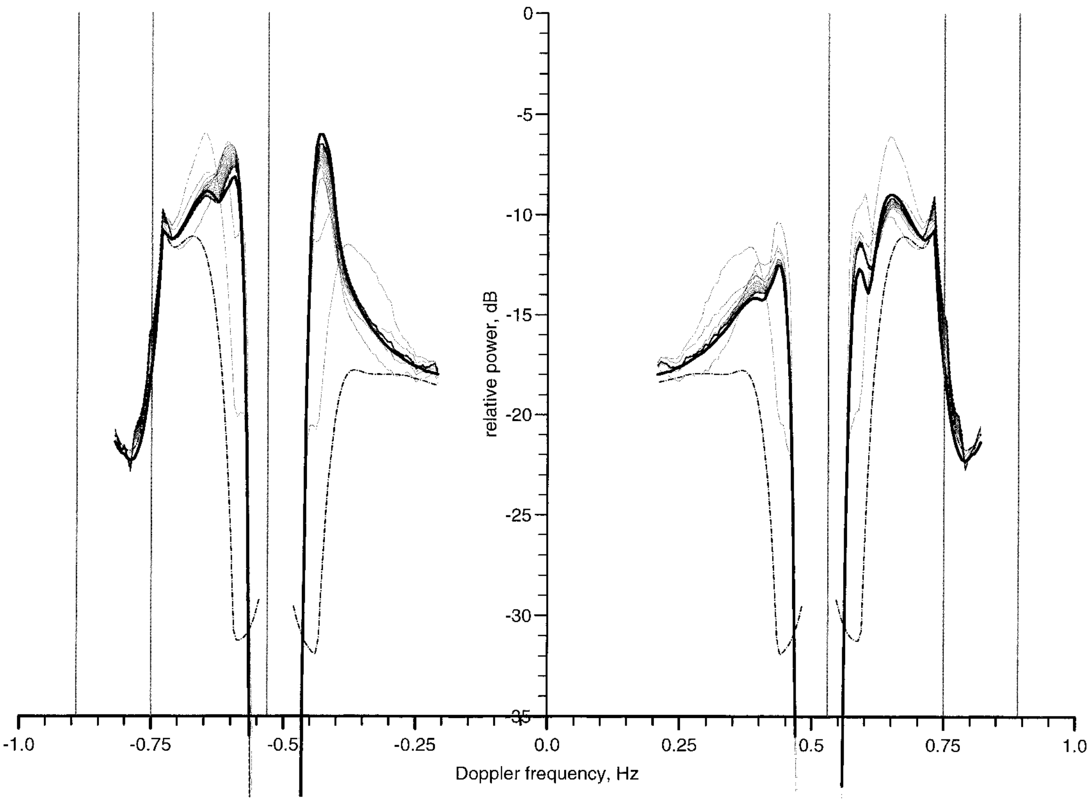

FIG. 3. The development of the Doppler spectrum through the iteration. The second-order sidebands for both radars are shown together by reversing the Doppler frequency range of the second radar, since its upper sidebands are also at negative Doppler frequencies. The solid black line shows the simulated spectra. This should be compared with the Doppler spectrum obtained at the end of the inversion, shown with the thicker dashed line. The dot-dashed line is the Doppler spectrum obtained using the initializing wave spectrum, that is, the starting point for the inversion. All others are at intermediate iterations. The vertical lines mark the position of the first-order peak (between each sideband), the $\sqrt{2}$ hydrodynamic, and the $2^{0.75}$ electromagnetic singularities.

tween the power spectrum of the demodulated backscattered signal and the ocean directional wavenumber spectrum. To first order, this takes the form

$$\sigma_1(\omega, \phi, d) = 2^6\pi k_0^4 \sum_{m'=\pm 1} S(-2m'\mathbf{k}_0)\delta(\omega - m'\omega_b), \tag{1}$$

where m' denotes the sign of the Doppler shift, $\mathbf{k}_0$ is the radar wave vector of magnitude k_0 and direction toward the scattering patch from the radar, $S(\mathbf{k})$ is the ocean directional wavenumber spectrum, $\omega_b = \sqrt{2gk_0\tanh(2k_0d)}$, and d is the water depth. This equation describes two peaks located at $\pm\omega_b$ with amplitudes dependent on the amplitudes in the directional spectrum along the radar beam direction toward, $S(-2\mathbf{k}_0)$, and away, $S(+2\mathbf{k}_0)$, from the radar.

The second-order contribution to the radar cross section is given by

$$\sigma_2(\omega, \phi, d) = 2^6\pi k_0^4 \sum_{m,m'=\pm 1} \int_{-\infty}^{+\infty}\int_{-\infty}^{+\infty} |\Gamma_T|^2 S(m\mathbf{k})S(m'\mathbf{k}')\delta[\omega - m\sqrt{(gk\tanh kd)} - m'\sqrt{(gk'\tanh k'd)}]\, dp\, dq, \tag{2}$$

where the integration variables, p and q, are wavenumber components parallel and perpendicular to $\mathbf{k}_0$, respectively, and are related to the three wave vectors, $\mathbf{k}$, $\mathbf{k}'$, and $\mathbf{k}_0$, by $\mathbf{k} = (p - k_0, q)$ and $\mathbf{k}' = (-p - k_0, -q)$ so that $\mathbf{k} + \mathbf{k}' = -2\mathbf{k}_0$. Here, m and m' (both equal to ± 1) locate the second-order contribution either to the left or the right of the first-order peaks. The term Γ_T is the coupling coefficient describing both the electromagnetic and hydrodynamic processes that provide the second-order backscatter. The details can be found in Holden and Wyatt (1992).

Equations (1) and (2) both have to be multiplied by

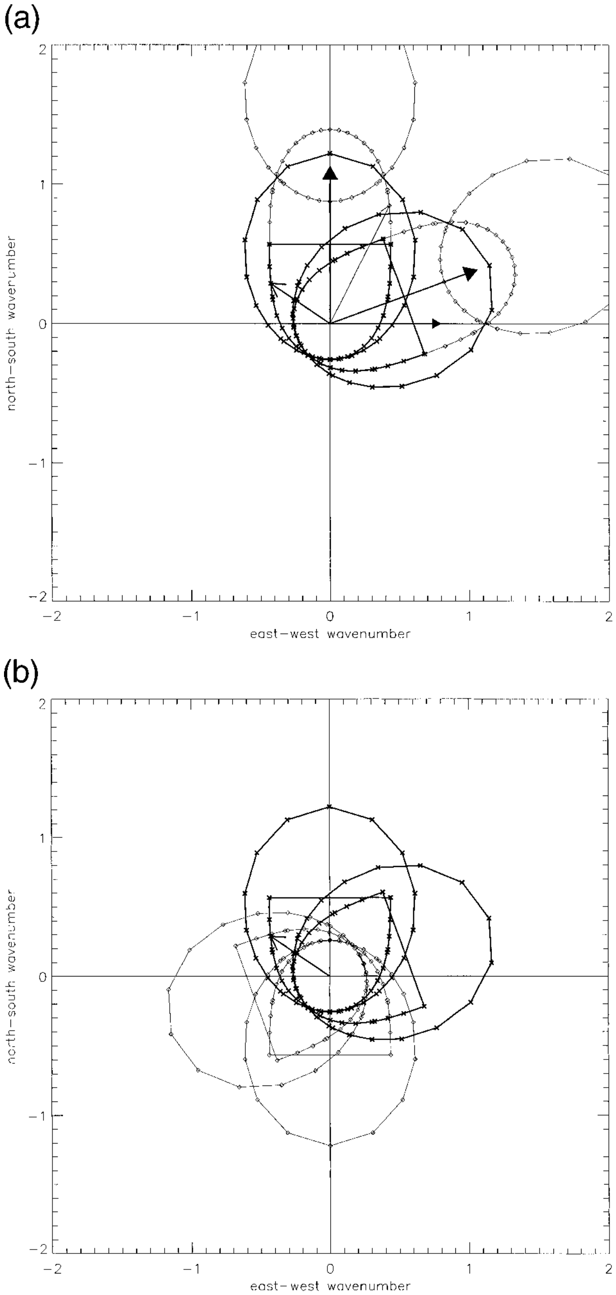

FIG. 4. Wavenumber ranges included in the case 5–8 inversions, (a) for the nonlinear case and (b) for the 8-sb linear inversion. Wavenumbers, for the Doppler frequency farthest from the first-order peaks for each sideband, are joined together to reveal the outer Doppler contour in each case. The darker lines show the $m\mathbf{k}$ vectors used in the linear inversion. The $m'\mathbf{k}'$ vectors to be included in the nonlinear inversion (a) and the $m\mathbf{k}$ vectors for the lower sidebands (b) are shown with lighter lines. The discretized wavenumbers themselves are shown with the symbol $\times$ for the $m\mathbf{k}$ vectors and $\diamond$ for the $m'\mathbf{k}'$ vectors. The horizontal axis measures the east–west component of the wave vectors, and the vertical axis measures the north–south component. Arrows with open arrowheads indicate sample vectors. Since m and m' are both negative for this example, these wave vectors sum to give the Bragg matched wave vector, $2\mathbf{k}_0$, shown for both radar look directions, with the large solid arrowheads in (a). The smaller solid arrow head in (a) shows wind direction for cases 5–8.

various radar parameters for a quantitative comparison with measured radar backscatter spectra. These are not always known. To avoid this problem, Eq. (2) is divided by Eq. (1) [or more usually by the integral of Eq. (1) over the finite width of the Bragg peak]. A large number of comparisons between the Doppler spectrum obtained by integrating the equation for a given ocean wave spectrum measured using a buoy and the Doppler spectrum measured by the radar at the location of the buoy have been made. In many sea states, the theory clearly provides a very good description of the backscatter, and it is this agreement that has motivated attempts to invert the equation.

Measurements with the PISCES radar during a storm showed that the equation does not do a good job of describing the backscatter at the peak of the storm (Wyatt 1995a). Backscatter measured using a radar beam looking into (or away from) the wind direction is significantly enhanced at second-order Doppler frequencies over the backscatter that would be predicted using Eq. (2). Recent measurements with the OSCR and WERA radars confirm that this effect occurs at lower sea states at the higher operating frequency (Wyatt 1998). Wyatt (1995a) reported that the breakdown of the theory depended on the directional properties of the wave spectrum, and these effects are also seen in the OSCR and WERA data. Figure 1 shows an OSCR example. In lower sea states (Fig. 1a) and in radar look directions more perpendicular to the wind direction (Figs. 1b,d), the second-order theory is in much better agreement with the measurements then is the case for the Doppler spectrum shown in Fig. 1c, measured with the relatively high waves (3 m significant wave height) propagating toward the radar. Recent work (Kingsley et al. 1998) has described the shape of the WERA Doppler spectrum as sea state increases when looking roughly into the wind and has shown that the slope of the second-order spectrum appears to saturate at a significant wave height of about 4 m. The consequences for the accuracy of wave measurements are described in Wyatt et al. (1999). The main effect is an overestimation of short wave amplitude, and until a new theory emerges, this can probably be dealt with by imposing a wave height dependent upper limit on the range of ocean wave frequencies for which the inversion is carried out. The alternative is to use a lower radio frequency where saturation will occur at a higher significant wave height.

b. The inversion problem

The normalized equation is used for wave measurement. It is a nonlinear, first kind Fredholm equation with a number of attendant numerical difficulties not least of which is the nonlinearity. Four methods that attempt a solution to this equation have been developed. Three of these are linearized methods—Lipa (1977), Wyatt (1990a), and Howell and Walsh (1993). These will be referred to as BL, LW, and HW, respectively. Of these,

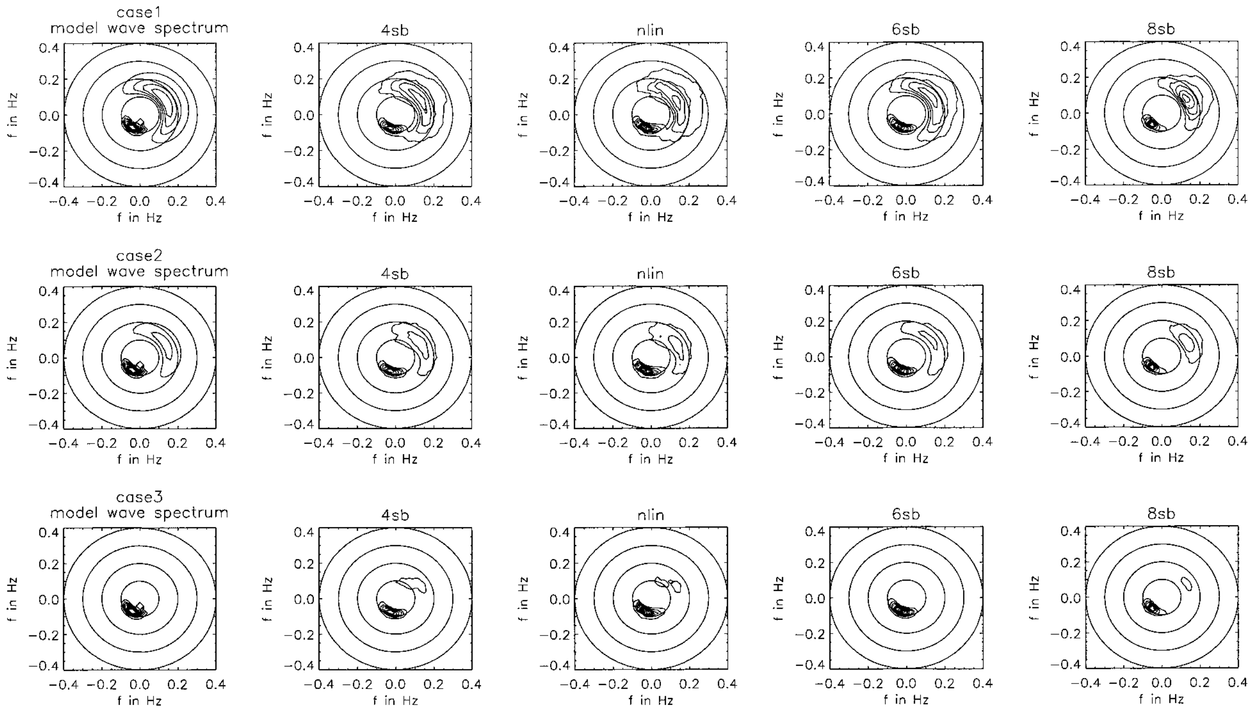

FIG. 5. The directional spectrum plotted in polar form, as in Fig. 2, with the model spectrum used in the simulation on the left and those obtained for the 4 sb, the nonlinear, the 6 sb, and the 8 sb inversions from left to right. Cases 1–3 are shown here.

BL and HW find a solution for the first five Fourier coefficients of the directional distribution, and LW finds the directional wavenumber spectrum on a wavenumber grid. The fourth, and most recently published, method is an optimization technique developed by Hisaki (1996) to solve the nonlinear problem. The LW method makes use of Doppler spectra measured at the same location from different directions using two radar systems. The PISCES, WERA, and OSCR systems have all been developed as dual-radar systems to avoid problems of direction and amplitude ambiguities that can otherwise arise. The HW and Hisaki methods can be used with either a dual-radar or a single-radar system but in the latter case, provide a reduced range of parameters, and the accuracy of these have not been published.

The LW method has been subject to exhaustive testing (Atanga and Wyatt 1997; Wyatt 1990b, 1991, 1995b; Wyatt and Holden 1992, 1994; Wyatt and Ledgard 1996; Wyatt et al. 1999; Krogstad et al. 1999), and good accuracy in a range of wave parameters determined from the directional spectrum has been demonstrated.

c. Linearizing methods

Close to the first-order Bragg peaks, the second-order backscatter is generated by combinations of long waves propagating in all directions with waves of the same order and propagating in roughly the same direction as the first-order Bragg wave. These short waves can, except in very low sea states, be assumed to be wind driven and hence modeled with a wind–wave model. This can take the form of a k^{-4} or f^{-5} (or similar) wavenumber or frequency model, as is used in the BL and HW inversions, or by using a Pierson–Moskowitz spectrum as is used in the LW model. In the latter case, additional information is required to provide the spectral peak. This is achieved using significant wave height and mean period found directly from the radar spectrum (Wyatt et al. 1985) to determine a wind speed and hence the spectral shape. In addition, a model of the directional distribution is required. In the BL and HW inversions, all short waves are assumed to be in the same direction as the first-order waves so the directional distribution cancels when the second order is scaled by the first order. The LW inversion extends the range of Doppler frequencies used and accounts for the resulting increased range in directions of the short-wave components by using a cardioid directional distribution around the mean direction determined from the first-order peaks using the same cardioid distribution. A method to estimate the parameters of a short-wave directional model has been developed (Wyatt et al. 1997) but is not yet implemented as part of the inversion.

These two-scale models apply over limited Doppler frequency ranges. The inversion should be limited to normalized Doppler frequencies, $\eta = \omega/\omega_b$, with $0.6 < |\eta| < \sqrt{2}$ in deep water. This frequency range reduces as the water depth decreases (Holden and Wyatt 1992). Beyond this, there are wavenumbers, $\mathbf{k}$, contributing to $S(\mathbf{k})$ that are of the same order as wavenumbers, $\mathbf{k}'$,

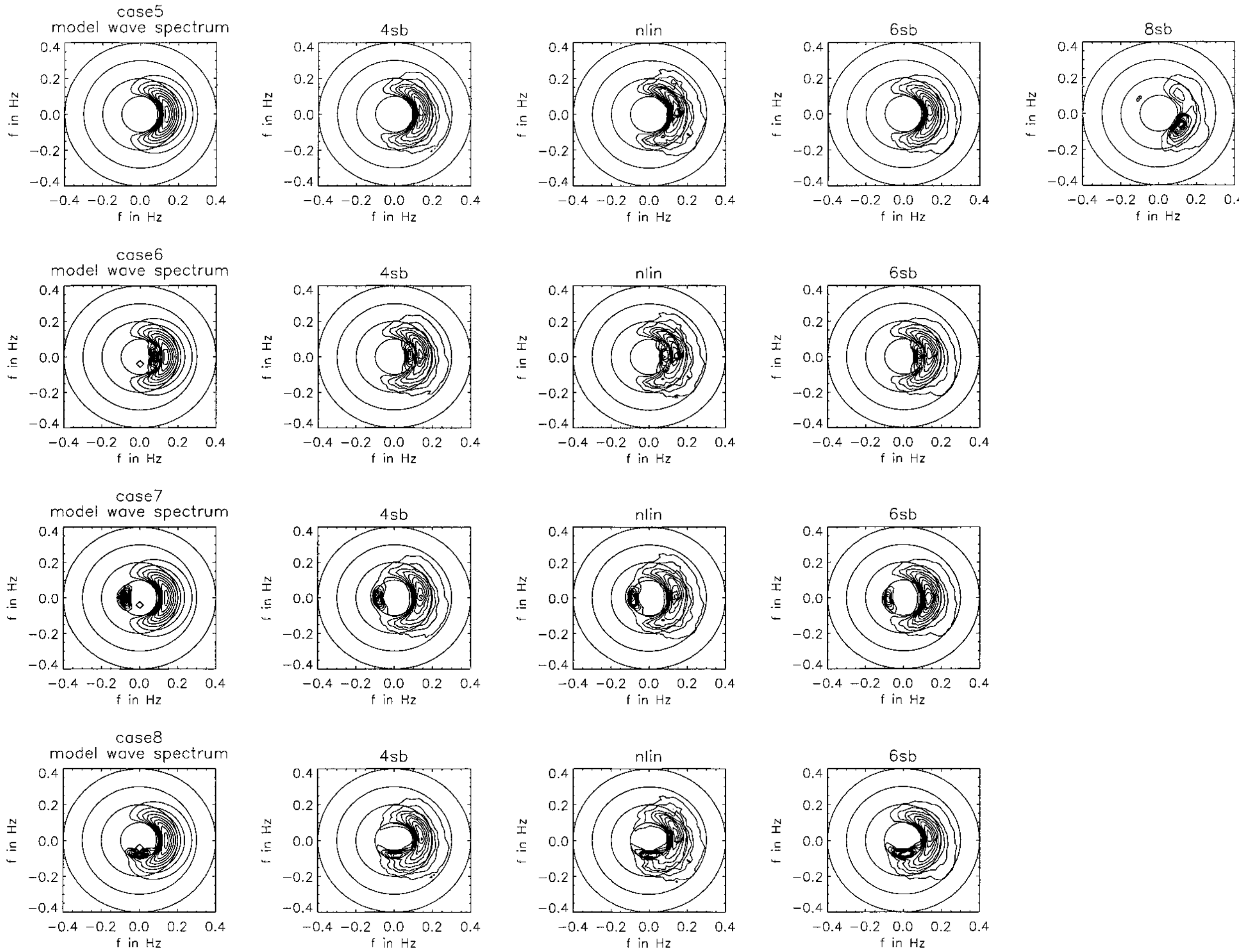

FIG. 6. As in Fig. 5 but for cases 5–8. No 8 sb inversion possible for cases 6–8.

contributing to $S(\mathbf{k}')$ either at the same or at different Doppler frequencies. Nonetheless, the LW method is applied over a Doppler frequency range $0.4 < |\eta| < 1.6$ with the assumption that the Pierson–Moskowitz spectrum will give a reasonable model of the longer wavelengths in $S(\mathbf{k}')$.

d. LW linear inversion method

This method is described in detail in Wyatt (1990a) and Atanga and Wyatt (1997). It is an iterative scheme that solves the direct problem, that is, it integrates Eq. (2) for a given wave spectrum at each iteration and then modifies the wave spectrum at each wavenumber according to the difference between the measured and integrated Doppler spectra at Doppler frequencies influenced by the wavenumber, weighted by the contribution that wavenumber makes relative to all other wavenumbers that contribute at the Doppler frequency. The wavenumbers used in this process are sampled at $\sim 15°$ intervals along the Doppler frequency contours determined by Eq. (3) and the radar signal spectral analysis, which sets the discretization of Doppler frequency. An inital wave spectrum, $S_0(\mathbf{k})$, is required, and for this, $S(\mathbf{k}')$ is used. The integrations are carried out for each frequency bin within the limited Doppler frequency ranges referred to above and are restricted to the two sidebands surrounding the larger Bragg peak for each of two radar measurements from the same location. To ensure that information from more than one sideband and more than one radar are used in the solution for each wavenumber, nearest neighbors from the other sideband and radar are identified and used in the adjustment process. These nearest neighbors identify the Doppler frequency, wavenumber, and propagation direction of the wave closest to the wavenumber vector whose amplitude is being adjusted. The method has been successfully applied to data collected at a range of radio frequencies (e.g., Wyatt and Holden 1992; Wyatt and Ledgard 1996; Wyatt et al. 1999). The range of Doppler frequencies used limits the range of ocean wave frequencies for which a solution is found. At 9 MHz, the upper limit is about 0.3 Hz, and at 27 MHz, about 0.38 Hz.

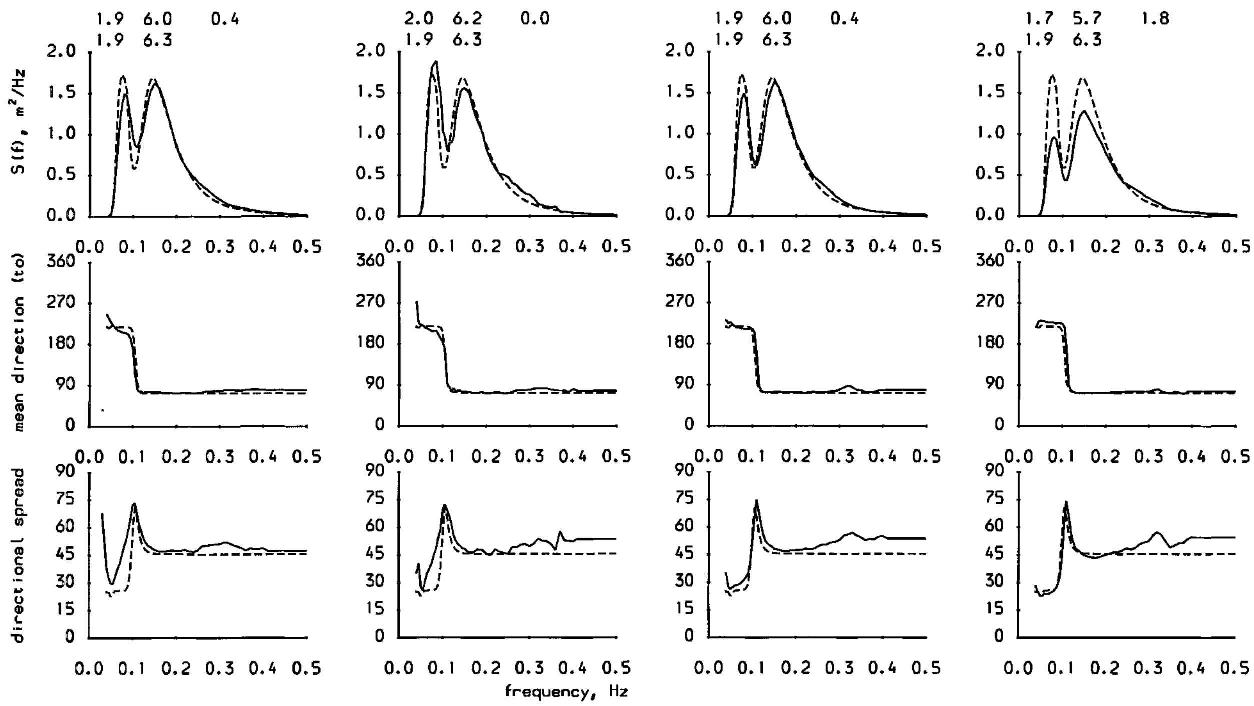

FIG. 7. Parametric plots of directional spectra for case 1 in the same order as Fig. 5. The inverted spectrum is shown with a solid line and the simulated spectrum with a dashed line. Above the plots are two rows of figures giving in the first row inverted wave height, mean period, and a quantity measuring the degree of convergence (<1 is usually a good inversion) and in the second row, the wave height and period of the simulated spectrum.

2. Linear inversion modifications

Two minor modifications to the numerical method are described here first. Of more importance is the discussion in section 2c about the extension of the method to make use of the second-order sidebands surrounding the lower Bragg peak.

a. Initializing spectrum

During the iterations, the modification procedure increases amplitude at a particular vector wavenumber according to the contribution of that wavenumber to the Doppler frequency when there is a difference in the inverted and simulated (or measured) Doppler spectra. But this increase is proportional to the existing amplitude. Since the initial spectrum that has been used is a pure wind–wave spectrum, if there is swell in the measured (or simulated) spectrum in a very different direction from the wind–wave mode, the larger initial amplitudes at all wavenumbers in the wind–wave direction (even though amplitudes at swell frequencies are initially very small) drive the initial swell mode development in this direction. The amplitude of the integral equation kernel at a particular wavenumber only takes over and corrects the swell direction later in the procedure. This slows down the convergence.

To improve convergence, the initializing spectrum has been modified in the following way. The wind–wave mode is determined as before, but amplitudes at all wavenumbers (in all directions) less than one half of the peak wavenumber in the Pierson–Moskowitz spectrum are initialized with values equal to the value at one half the peak wavenumber in the wind–wave direction. There is thus a uniform plateau from which the swell mode can grow. Figure 2 shows the development of the swell mode as the iteration proceeds with reasonable agreement between inverted and simulated spectra after 20 iterations. The convergence of the corresponding Doppler spectrum is seen in Fig. 3.

b. Convergence criterion

The quantity used to determine convergence measures the mean difference in dB between the inverted (at each

→

FIG. 8. Doppler spectrum plots (as in Fig. 3) comparing the final Doppler spectra for the linear (dotted line), 6 sb (dashed), and 8 sb (dash-dot) inversions with the simulated spectrum (solid). The nonlinear spectrum is also plotted (spaced dots) but is barely seen in this case, since it is almost the same as the simulated spectrum. Here (a) is for the first radar and (b) for the second radar.

(a)

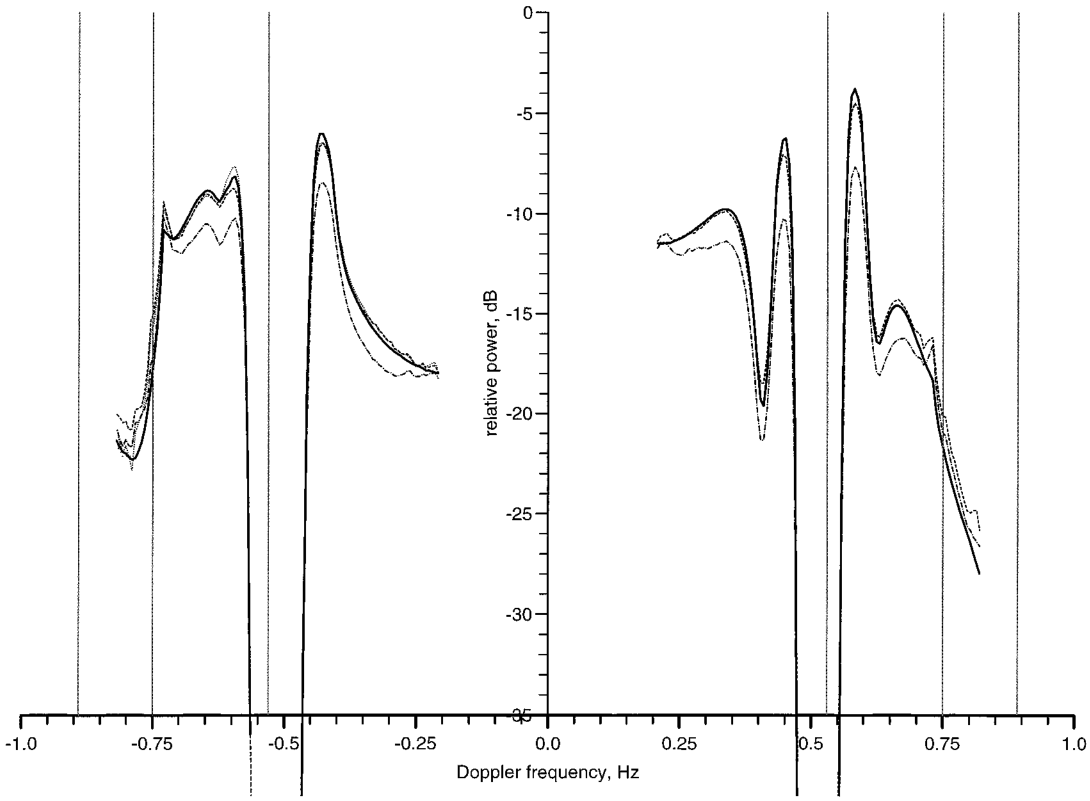
0
-5
-10
-15
-20
-25
-30
-35
relative power, dB
-1.0
-0.75
-0.5
-0.25
0.0
0.25
0.5
0.75
1.0
Doppler frequency, Hz

(b)

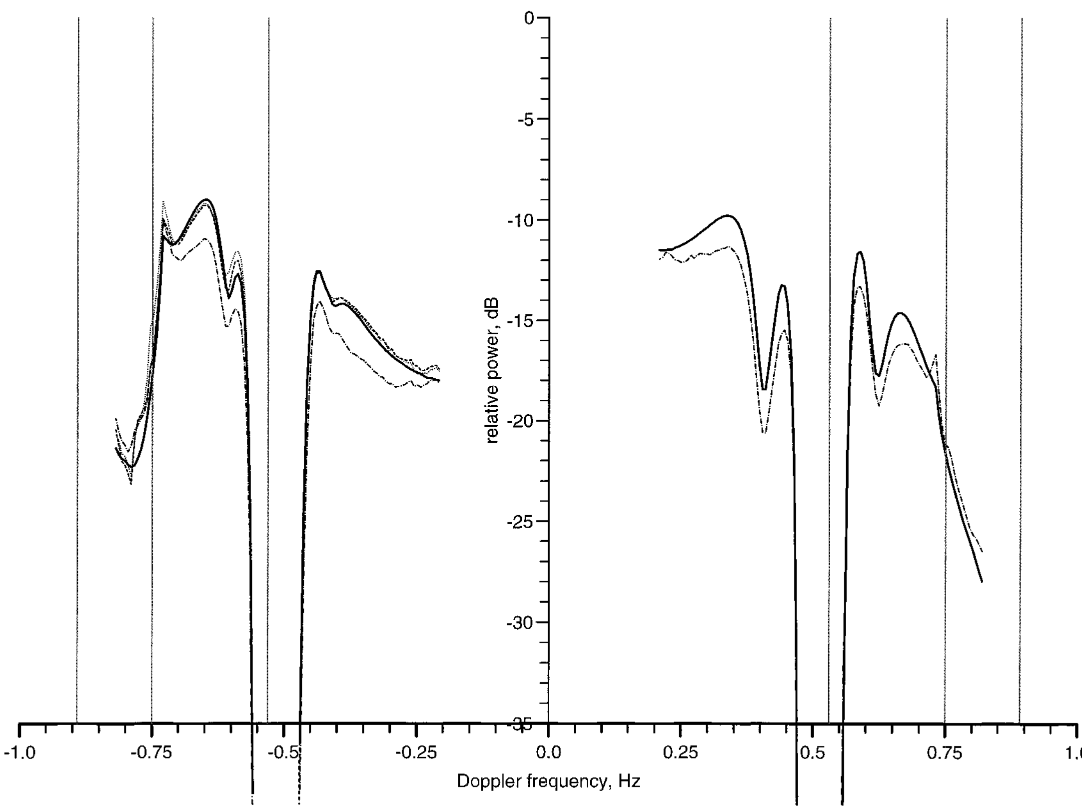
0
-5
-10
-15
-20
-25
-30
-35
relative power, dB
-1.0
-0.75
-0.5
-0.25
0.0
0.25
0.5
0.75
1.0
Doppler frequency, Hz

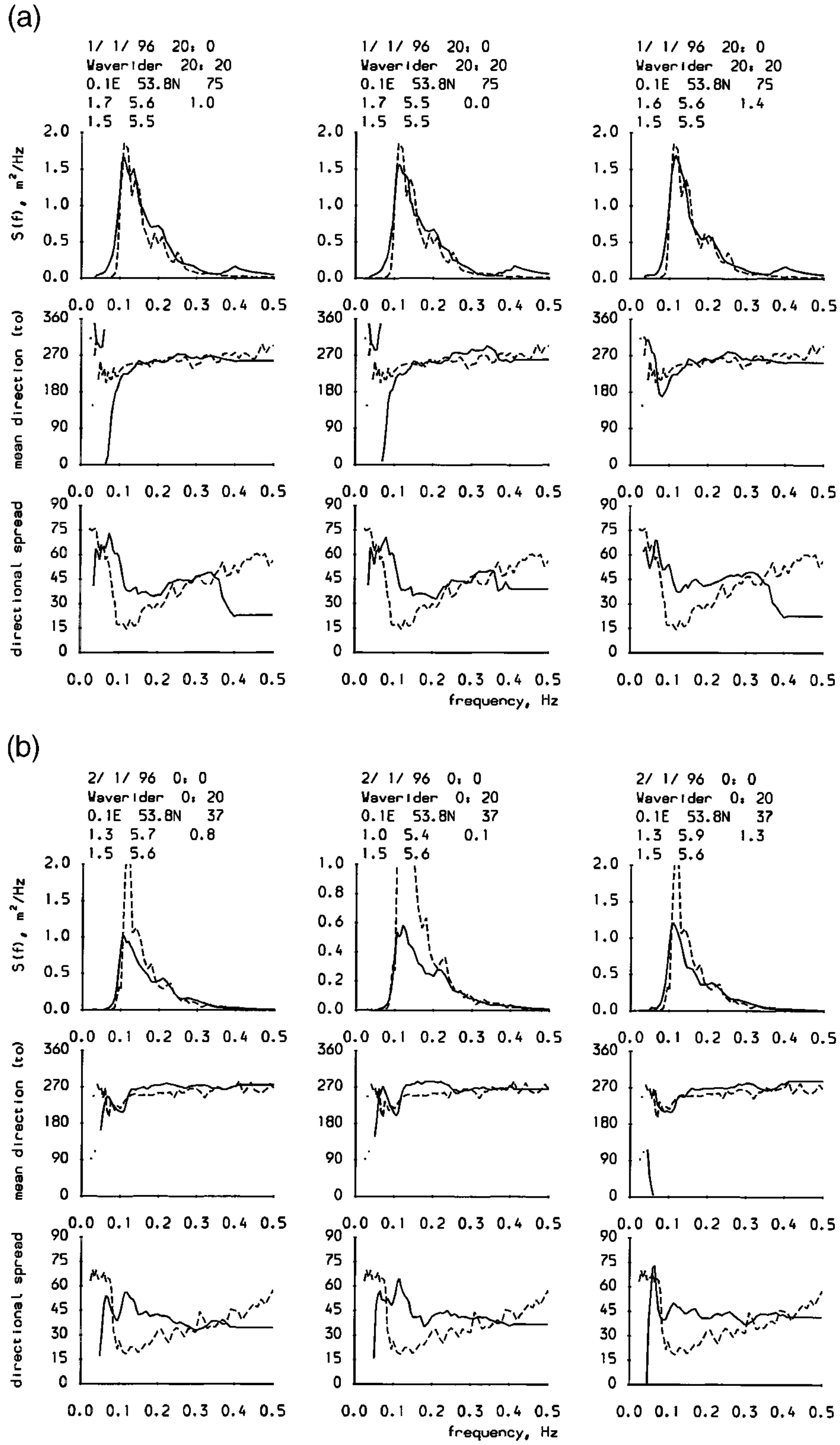

FIG. 9. The directional spectrum measured by OSCR during Holderness is plotted in parametric form, the inversion is the solid line and the wave buoy data the dashed line. The date, time, and location of the two measurements are shown. Beneath these are two rows of figures giving in the first row radar wave height, mean period, and a quantity measuring the degree of convergence (<1 is usually a good inversion) and in the second row, the wave height and period of the buoy measurement. The linear inversion is on the left followed by the nonlinear and 6 sb inversions.

iteration) and the measured spectrum over the Doppler frequency range being modified. The convergence criterion has been modified to account for subtle but important changes to the directional spectrum in the later stages of the inversion. Two quantities are monitored. One, c_1, is the mean difference described above but summed over the last two iterations to smooth small fluctuations. The second, c_2, is the absolute difference between c_1 measured at the current iteration with that measured at the last. Convergence is assumed to have occurred if either $c_1 < 0.5$ dB or $c_2 < 0.001$ dB.

c. Using the lower Bragg peak sidebands

A recent comparison between the performance of the LW and HW methods (Atanga and Wyatt 1997) has suggested that using the second-order sidebands around both first-order peaks when signal-to-noise is sufficient might improve the accuracy of the inversion. The HW method performed significantly better in amplitude estimation in these circumstances, which tend to be cases where the wind direction is roughly perpendicular to one of the radar beams. The LW method has been extended to include this part of the spectrum, provided the signal-to-noise there is greater than 15 dB, the same criterion as is used for the larger sidebands. However, this signal-to-noise criterion was not found to be sufficient. A criterion based on comparing the integrated amplitude in the Doppler spectrum normalized to the integral under the larger peak proved to be the most reliable, although further work is needed to confirm that this is universally applicable. When this ratio falls below about 10%, use of the additional sidebands increases rather than decreases the error in the inversion. This is because the lower sideband amplitudes are rather sensitive to the relative amplitudes of the two Bragg peaks and hence to wind direction. This is less of a problem for simulated cases, where the estimated wind direction, obtained by combining the estimates from each simulated Doppler spectrum, is rather accurate. However, for the measured cases, the individual Doppler spectra usually do not produce exactly the same estimate of wind direction, and an average is used. This has only a very small effect on the upper sideband amplitudes but can lead to large differences for the lower sidebands.

The results obtained provide some evidence that improvement in accuracy might be possible with this extension, although this improvement is not very large for the cases considered so far. If the technique is to be applied for operational applications, a detailed statistical analysis is needed using one or more of the many datasets that have been used in the evaluation of the existing inversion method. However, the small improvements that might be delivered may not be worth the additional computing resource required.

The results are presented alongside the nonlinear results in section 5. In some of the cases considered, the signal-to-noise requirement means that additional sidebands are only used from one of the radars. In general, there are three possible combinations referred to as 4 sb (two sidebands from each radar), 6 sb (four sidebands from one radar), and 8 sb, where all sidebands are of sufficient signal-to-noise to be used.

3. Limitations to linear and nonlinear inversion

The difficulty with the inversion of Eq. (2) is that the problem is ill-posed, and therefore, any solution method has to impose constraints of some sort. The LW method works because each wavenumber, at which an inversion is attempted, contributes to more than one sideband, and preferably more than one radar spectrum and smoothing is introduced to keep the solution at each wavenumber tied to that of its nearest neighbors. The second radar is particularly important in this respect.

a. Wavenumber ranges

The wavenumbers that contribute to the range of Doppler frequencies used in the LW inversion can be determined using the delta function in Eq. (2),

$$\delta[\omega - m\sqrt{(gk \tanh kd)} - m'\sqrt{(gk' \tanh k'd)}], \qquad (3)$$

together with the second-order Bragg condition $\mathbf{k} + \mathbf{k}' = -2\mathbf{k}_0$. This equation has different solutions for the different m, m' combinations and for each of the two radar directions, $\mathbf{k}_0$, used in the dual-radar solution. Figure 4a shows the wavenumber ranges that are included in the inversion for one particular radar direction pair (separated by 70° in this case). Note that it is $m\mathbf{k}$ (thick line and $\times$ marking each discretized wavenumber used) and $m'\mathbf{k}'$ (thin line and $\diamond$) that are plotted here, since it is at these wave vectors that adjustments are being made during the inversion. The plots show the Doppler contour farthest from the first-order peaks. Other contours are similar in shape within these limits. Because $m\mathbf{k}$ and $m'\mathbf{k}'$ are included here separately, there are four contour groupings for each radar. An example of a $m\mathbf{k}$, $m'\mathbf{k}'$ pair is shown with arrows.

The linear inversion method estimates the spectrum at all wavenumbers $m\mathbf{k}$, within the limits shown on the diagram, that have near neighbors from one of the other sidebands (from the same or the other radar). The spectrum at all other wavenumbers is estimated using the initializing Pierson–Moskowitz spectrum. The wind direction used in the initialization for this wavenumber set is shown in Fig. 4a. It can be seen here that the only part of the wavenumber plane that is covered over the full 0–2π range is the long wavenumber range (close to the origin). Over most of the plane, the range of directions is limited. For this particular configuration, full directional coverage is limited to wavenumbers less than about 0.3 m^{-1} ($\sim$0.27 Hz). This is less than the frequency range used in the inversion, and clearly at higher frequencies, some reduction in accuracy can be expected. However, this is ameliorated to a certain ex-

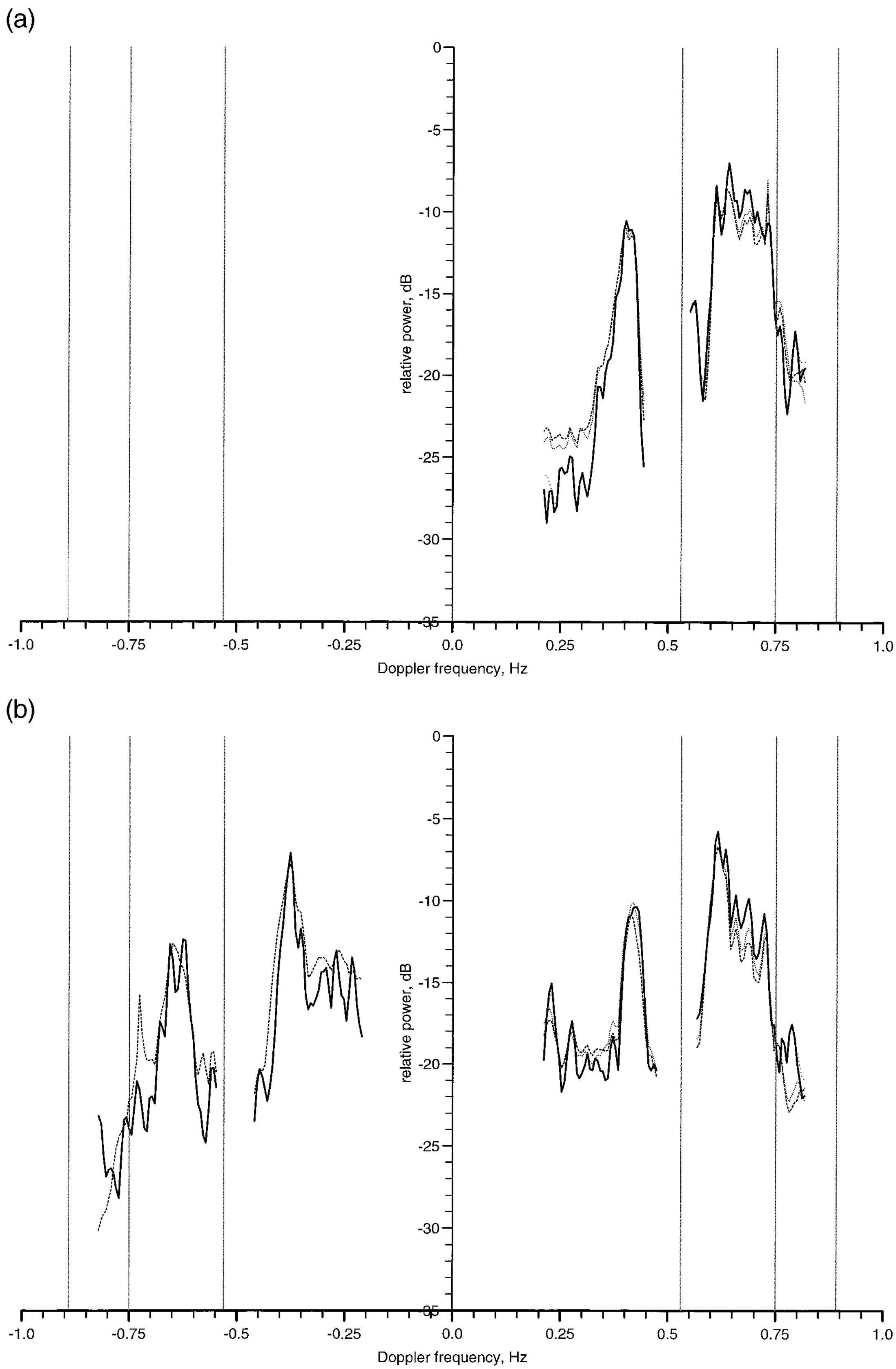
(a)
relative power, dB
0
-5
-10
-15
-20
-25
-30
-35
-1.0
-0.75
-0.5
-0.25
0.0
0.25
0.5
0.75
1.0
Doppler frequency, Hz
(b)
relative power, dB
0
-5
-10
-15
-20
-25
-30
-35
-1.0
-0.75
-0.5
-0.25
0.0
0.25
0.5
0.75
1.0
Doppler frequency, Hz

tent because, as can be seen in Fig. 4a, the high frequencies included in the inversion are those in the half plane containing the wind direction. So it is only the spectrum at high frequencies opposed to the wind direction, where energy levels should be low, that is not part of the inversion. This reduction in accuracy at higher frequencies will also be present in other inversion methods that limit the Doppler frequency range (as all of the existing ones do).

A nonlinear inversion will provide estimates of the directional spectrum at $m\mathbf{k}$ and at $m'\mathbf{k}'$. Therefore, of concern here is the location of the contributions from $m'\mathbf{k}'$. As can be seen in the figure, there is considerable overlap between the $m'\mathbf{k}'$ contribution to the outer sideband and the $m\mathbf{k}$ contribution to the inner sideband of the same radar. There is some overlap between the $m'\mathbf{k}'$ contributions to both sidebands. There is only a very limited overlap between $m'\mathbf{k}'$ contribution to the outer sideband of one radar with the $m\mathbf{k}$ contribution to the inner sideband of the other radar and no overlap between $m'\mathbf{k}'$ contribution to the inner sidebands of the two radars. There is very limited coverage of the full direction range for any of these cases. Again, this will be a problem for any inversion method that restricts the range of Doppler frequencies used.

Thus it is anticipated that the accuracy of a nonlinear inversion, restricted to the same Doppler frequency range, will be limited particularly by the lack of overlap in high wavenumber ranges between the two radars.

b. Doppler frequency ranges

Making use of a wider range of Doppler frequencies would increase the overlapped coverage of the wavenumber plane by the two radars. One extension, as has already been mentioned, is to include the Doppler frequencies around the weaker first-order peak, provided that signal-to-noise is sufficient. The coverage obtained is seen in Fig. 4b, which shows $m\mathbf{k}$ for an 8 sb linear inversion. The $m'\mathbf{k}'$ contours (not shown here), which would be used in a nonlinear inversion, can be easily assessed by comparing Figs. 4a and b. The range of wavenumbers that now have full directional coverage is more than doubled (to $\sim$0.8 m^{-1}), but there is very little additional overlap in directional coverage at high wavenumbers.

The other alternative is to extend the Doppler frequency range beyond $0.4 < |\eta| < 1.6$. The problem with this is that the numerical integration used in the direct part of the procedure becomes increasingly inaccurate as the inner sideband contours increase in size (measured by the wavenumber range covered). Secondly, as has been mentioned above, the second-order model becomes increasingly inaccurate as a description of the outer sideband, particularly at higher values of $|\eta|$ as wave height increases.

4. Nonlinear inversion method

a. Staged approach

In spite of all the anticipated limitations, a nonlinear method has been developed. The LW method requires that individual wavenumbers contribute to more than one sideband, and the limitations of this have already been referred to. Thus a three-stage approach has been adopted. Stage 1 is the same as the linear inversion, that is, $S(\mathbf{k})$ is modified, after the integration is carried out, in the way described before. At stage 2, $S(\mathbf{k})$ is modified for contributions to the inner sideband, but $S(\mathbf{k}')$ is modified for contributions to the outer sideband. In Fig. 4a, it can be seen that there is significant overlap between the wavenumbers involved here. Finally, at stage 3, $S(\mathbf{k}')$ is modified for both sidebands.

b. Nearest neighbors

In order to implement the modifications described in section 4a, nearest neighbors have to be determined for $\mathbf{k}$ and $\mathbf{k}'$ at stage 2 and for $\mathbf{k}'$ and $\mathbf{k}'$ at stage 3. At stage 3, the discretizations for the two sidebands produce wavenumber increments that are similar (distances between the $\diamondsuit$ symbols in Fig. 4a), as they were in stage 1. However, at stage 2, this is not the case. There are large variations in $\mathbf{k}$ but small variations in $\mathbf{k}'$ (compare distances between the $\times$ and the $\diamondsuit$ symbols), with the result that many $\mathbf{k}'$ will share the same nearest neighbor in $\mathbf{k}$. This is likely to have a smoothing effect in the solution.

c. Iteration scheme

Implementing the three-stage procedure from the outset of an inversion has not proved successful. Best results have been achieved when the linear inversion is allowed to iterate to convergence, at which stage the three-stage procedure is implemented. This iterates until the convergence criterion has been met (see section 2b). Criterion c_1 is modified to be the sum of Doppler spectral differences for the current and two previous iterations, that is, over three stages. Criterion c_2 has the same definition as before, and the same minimum values are required.

←

FIG. 10. Doppler spectrum plots for the second case in Fig. 9 again showing the linear (dotted) and the 6 sb (dashed) spectra compared with the measured (solid) Doppler spectrum for (a) radar 1 and (b) radar 2 (where both sidebands are used). The nonlinear spectrum is also plotted (spaced dots), but it is almost the same as the simulated spectrum and is only visible at the extreme Doppler frequencies.

5. Results

a. Simulations

Eight different ocean wave spectra have been used to generate simulated Doppler spectra to test the methods. This is not adequate to make a quantitative assessment of accuracy but is sufficient to demonstrate the nature of the solutions. One case is of a pure wind–wave spectrum, and in all the others, swell has been added with different relative amplitudes and directions. In all cases, a water depth of 20 m and a Pierson–Moskowitz wind–wave model have been used. For the swell cases, a peak frequency of 0.08 Hz has been used. The remaining parameters are shown in Table 1. The first four cases are those used in Atanga and Wyatt (1997).

Figures 5 and 6 show polar plots comparing the linear with the nonlinear solution and the solutions using additional sidebands from one and from both beams with the model spectrum used in the simulations. Case 4 is not included in the plot because it looks very similar to case 3. There is usually little difference between the 4 sb, the nonlinear, and the 6 sb cases, but the 8 sb cases are not as accurate. Case 5 (in Fig. 6) is one where the 8 sb inversion should not have been attempted because the amplitude ratio criterion for one of the radars was far from satisfied. The result is characteristic of the behavior of the inversion in such cases. The solution oscillates between two directional shapes, with the peak alternately to the northwest and southwest for this case. Figure 7 shows the results presented in parametric form for case one, with the frequency spectrum, mean direction, and spread as functions of frequency compared with the parameters of the spectra input to the simulations. These plots combine the wave spectrum obtained by inversion with the Pierson–Moskowitz spectrum model used at high frequencies, and hence the plots extend to 0.5 Hz. In this display, it is again difficult to distinguish between the 4 sb, the nonlinear, and the 6 sb solutions, although the 6 sb case slightly has the edge in directional spread accuracy at low frequencies. It is clear here that the 8 sb case does not get the amplitudes as accurately. This was more difficult to see in the polar comparisons. Figure 8 shows the part of the normalized Doppler spectra used in the inversions compared with the normalized Doppler spectra obtained using the inverted wave spectra (i.e., the last direct calculation done before convergence) for all four solutions again for case 1. While the differences are quite small (apart from the 8 sb case), the nonlinear solution does provide a better fit to the simulated spectra, so much so that it can hardly be seen in the plot. Presumably, the fact that this does not also result in a more accurate solution for the wave spectrum is associated with the problems of coverage of the wavenumber plane already referred to.

b. OSCR data

The OSCR measurements were made at the location of a directional waverider during the second Holderness experiment (Prandle et al. 1996). It is much more difficult to find cases where the amplitude ratio criterion for 6 sb or 8 sb inversions is satisfied and the evidence for any improvement is not clear. A much more detailed analysis is required along the lines already used to evaluate the 4 sb case (Wyatt et al. 1999). Furthermore, it is more difficult to compare spectral shape because the waverider provides only a parameterized form of the directional spectrum. The use of the maximum entropy method to estimate the directional spectrum from these parameters has been shown to be useful (Krogstad et al. 1999) but is not completely satisfactory when it comes to looking for small differences between the different inversions. Two cases are shown in Fig. 9 in parametric form. The 6 sb inversion for the first example is perhaps slightly better. As was the case with the simulations, the nonlinear inversion generates a Doppler spectrum that is closer to the measured spectrum, although the wave spectrum is not as accurate. Figure 10 shows one such example where again it is difficult to see the nonlinear case, since it is almost aligned with the measured Doppler spectrum.

6. Discussion

Two extensions to the LW method for determining the ocean wave directional spectrum from HF radar backscatter have been presented. One concerns the use of the lower second-order sidebands in the analysis when there is sufficient signal-to-noise and has shown small improvements in the accuracy of the estimated wave spectrum. The statistical significance of these improvements and the exact signal-to-noise criteria required to implement the method need further work. The lower sidebands are vulnerable to contamination due to antenna sidelobes, to short timescale current variability, and probably other hydrodynamic effects not accounted for in the backscatter modeling. This may explain why the application to OSCR data is less robust than the application to simulated data.

It has been demonstrated that the LW linear inversion method can be extended to a nonlinear solution, that is, to a solution that provides an estimate of both the long- and short-wave parts of the wave spectrum. This nonlinear solution does indeed generate Doppler spectra that converge to measured or simulated spectra better than is achieved using the linear method. However, this does not result in a more accurate ocean wave directional spectrum probably because the inversion at high wavenumbers only covers a small range of directions.

Of more practical importance is the observation in section 1a and Fig. 1 that the Doppler spectrum does not conform to second-order theory in high sea states when the radar is looking into the wind. A different theoretical formulation is required to deal with this situation. This problem is more serious at the high HF operating frequencies of the OSCR and WERA radar systems, since it starts to become a problem at significant wave heights above about 3 m (as seen in Fig. 1c). The alternative is to use lower radio frequencies. The PISCES measurements were made to significant wave heights over 7 m, with no significant effect on accuracy due to this limitation. Theory would suggest (Wyatt 1995a) that problems would start to arise at wave heights in excess of about 10 m at PISCES operating frequencies.

The OSCR and WERA deployments have shown that the inversion (whether linear with additional sidebands or nonlinear) overestimates amplitudes at higher ocean wave frequencies in these circumstances, although directions are, on the whole, recovered well (Wyatt et al. 1999). The increased power in the measured Doppler spectum is converted into increased energy in the wave spectrum in the corresponding frequency range. One method that could be used to avoid the problem is to set a maximum ocean wave frequency for the inversion in inverse proportion to significant wave height. This would limit the opportunity to observe the development of new wave systems when the overall sea state remains high, although perhaps this is not a serious practical limitation.

Acknowledgments. This work has been partly supported by EPSRC (GR/J07341), NERC (F3CR07-G1-02), and EU (MAS2-CT94-0103). I am very grateful to the anonymous referees for many helpful comments.

REFERENCES

Atanga, J., and L. R. Wyatt, 1997: Comparison of inversion algorithms for HF radar wave measurements. *IEEE J. Oceanic Eng.,* **22,** 593–603.

Barrick, D. E., 1971: Theory of HF and VHF propagation across the rough sea. Part II. *Radio Sci.,* **6,** 527–533.

——, 1972: First-order theory and analysis of MF/HF/VHF scatter from the sea. *IEEE Trans. Antennas Propag.,* **AP-20,** 2–10.

——, and B. L. Weber, 1977: On the nonlinear theory for gravity waves on the ocean's surface. Part II: Interpretation and applications. *J. Phys. Oceanogr.,* **7,** 11–21.

Crombie, D. D., 1955: Doppler spectrum of sea echo at 13.56Mc/s. *Nature,* **175,** 681–682.

Gurgel, K.-W., G. Antonischki, H.-H. Essen, and T. Schlick, 1999: Wellen Radar (WERA): A new ground-wave HF radar for ocean remote sensing. *Coastal Eng.,* **37,** 219–234.

Hisaki, Y., 1996: Nonlinear inversion of the integral equation to estimate ocean wave spectra from HF radar. *Radio Sci.,* **31,** 25–39.

Holden, G. J., and L. R. Wyatt, 1992: Extraction of sea state in shallow water using HF radar. *IEE Proc.-F,* **139,** 175–181.

Howell, R., and J. Walsh, 1993: Measurement of ocean wave spectra using narrow beam HF radar. *IEEE J. Oceanic Eng.,* **18,** 296–305.

Kingsley, S. P., A. M. Torregrossa, and L. R. Wyatt, 1998: Analysis of second order HF radar sea spectra recorded in storm conditions. *Proc. Oceans '98,* Nice, France, IEEE, 459–462.

Krogstad, H. E., J. Wolf, S. P. Thompson, and L. R. Wyatt, 1999: Methods for the intercomparison of wave measurements. *Coastal Eng.,* **37,** 235–258.

Lipa, B. J., 1977: Derivation of directional ocean-wave spectra by inversion of second order radar echoes. *Radio Sci.,* **12,** 425–434.

——, and D. E. Barrick, 1986: Extraction of sea state from HF radar sea echo: Mathematical theory and modelling. *Radio Sci.,* **21,** 81–100.

——, ——, J. Isaacson, and P. M. Lilleboe, 1990: CODAR wave measurements from a North Sea semisubmersible. *IEEE J. Oceanic Eng.,* **15,** 119–125.

Paduan, J. D., and H. C. Graber, 1997: Introduction to High-Frequency radar: Reality and myth. *Oceanography,* **10,** 36–39.

Prandle, D., and Coauthors, 1996: The Holderness coastal experiment '93–'96. POL Rep. 44, Proudman Oceanographic Laboratory, Birkenhead, United Kingdom.

Rice, S. O., 1951: Reflection of electromagnetic waves from slightly rough surfaces. *Theory of Electromagnetic Waves,* Interscience and Dover, 351–378.

Robson, R. E., 1984: Simplified theory of first- and second-order scattering of HF radio waves from the sea. *Radio Sci.,* **19,** 1499–1504.

Shearman, E. D. R., and M. D. Moorhead, 1988: Pisces: A coastal ground-wave radar for current, wind and wave mapping to 200-km ranges. *Proc. IGARRS '88,* Edinburgh, Scotland, ESA Publications Division, 773–776.

Walsh, J., and S. K. Srivastava, 1987: Rough surface propagation and scatter, 1. General formulation and solution for periodic surfaces. *Radio Sci.,* **22,** 193–208.

Weber, B. L., and D. E. Barrick, 1977: On the nonlinear theory for gravity waves on the ocean's surface. Part I: Derivations. *J. Phys. Oceanogr.,* **7,** 3–10.

Wyatt, L. R., 1990a: A relaxation method for integral inversion applied to HF radar measurement of the ocean wave directional spectrum. *Int. J. Remote Sens.,* **11,** 1481–1494.

——, 1990b: Progress in the interpretation of HF sea echo 'clutter': HF radar as a remote sensing tool. *IEE Proc.-F,* **137,** 139–147.

——, 1991: HF radar measurements of the ocean wave directional spectrum. *IEEE J. Oceanic Eng.,* **16,** 163–169.

——, 1995a: High order nonlinearities in HF radar backscatter from the ocean surface. *IEE Proc. Radar Sonar Navig.,* **142,** 293–300.

——, 1995b: The effect of fetch on the directional spectrum of Celtic Sea storm waves. *J. Phys. Oceanogr.,* **25,** 1550–1559.

——, 1998: HF radar wave measurements in high sea-states. *Proc. Oceans '98,* Nice, France, IEEE, 463–466.

——, and G. J. Holden, 1992: Developments in ocean wave measurement by HF radar. *IEE Proc.-F,* **139,** 170–174.

——, and ——, 1994: Limits in direction and frequency resolution for HF radar ocean wave directional spectra measurement. *Global Atmos. Ocean Syst.,* **2,** 265–290.

——, and L. J. Ledgard, 1996: OSCR wave measurement—Some preliminary results. *IEEE J. Oceanic Eng.,* **21,** 64–76.

——, G. D. Burrows, and M. D. Moorhead, 1985: An assessment of a FMICW ground-wave radar system for ocean wave studies. *Int. J. Remote Sens.,* **6,** 275–282.

——, L. J. Ledgard, and C. W. Anderson, 1997: Maximum-likelihood estimation of the directional distribution of 0.53-Hz ocean waves. *J. Atmos. Oceanic Technol.,* **14,** 591–603.

——, S. P. Thompson, and R. R. Burton, 1999: Evaluation of HF radar wave measurement. *Coastal Eng.,* **37,** 259–282.